Influences of Ash-Existing Environments and Coal Structures on CO2 Gasification Characteristics of Tri-High Coal

Authors:

Lang Liu, Qingrui Jiao, Jian Yang, Bowen Kong, Shan Ren, Qingcai Liu

Date Submitted: 2021-05-17

Keywords: tri-high coal, coal structure, CO2 gasification, ash-free coal

Abstract:

Two kinds of tri-high coals were selected to determine the influences of ash-existing environments and coal structures on CO2 gasification characteristics. The TGA results showed that the gasification of ash-free coal (AFC) chars was more efficient than that of corresponding raw coal (RC) chars. To uncover the reasons, the structures of RCs and AFCs, and their char samples prepared at elevated temperatures were investigated with SEM, BET, XRD, Raman and FTIR. The BET, SEM and XRD results showed that the Ash/mineral matter is associated with coal, carbon forms the main structural framework and mineral matters are found embedded in the coal structure in the low-rank tri-high coal. The Raman and FTIR results show that the ash can hinder volatile matters from exposing to the coal particles. Those results indicate that the surface of AFC chars has more free active carbon sites than raw coal chars, which are favorable for mass transfer between C and CO2, thereby improving reactivity of the AFC chars. However, the gasification reactivity was dominated by pore structure at elevated gasification temperatures, even though the microcrystalline structure, functional group structure, and increase in the disorder carbon were improved by acid pickling.

Record Type: Published Article

Submitted To: LAPSE (Living Archive for Process Systems Engineering)

Citation (overall record, always the latest version):	LAPSE:2021.0368
Citation (this specific file, latest version):	LAPSE:2021.0368-1
Citation (this specific file, this version):	LAPSE:2021.0368-1v1

DOI of Published Version: https://doi.org/10.3390/pr8111367

processes

MDPI

Article

Influences of Ash-Existing Environments and Coal Structures on CO_2 Gasification Characteristics of Tri-High Coal

Lang Liu [1,*], Qingrui Jiao [2], Jian Yang [2], Bowen Kong [2], Shan Ren [2] and Qingcai Liu [2]

[1] Chemical Engineering Institute, Guizhou Institute of Technology, Guiyang 550003, China
[2] College of Materials Science & Engineering, Chongqing University, Chongqing 400044, China; 201809021080@cqu.edu.cn (Q.J.); skyinjune@cqu.edu.cn (J.Y.); BoWen.Kong@cisdi.com.cn (B.K.); shan.ren@cqu.edu.cn (S.R.); liuqc@cqu.edu.cn (Q.L.)
* Correspondence: l.liu@git.edu.cn

Received: 26 August 2020; Accepted: 24 October 2020; Published: 28 October 2020

Abstract: Two kinds of tri-high coals were selected to determine the influences of ash-existing environments and coal structures on CO_2 gasification characteristics. The TGA results showed that the gasification of ash-free coal (AFC) chars was more efficient than that of corresponding raw coal (RC) chars. To uncover the reasons, the structures of RCs and AFCs, and their char samples prepared at elevated temperatures were investigated with SEM, BET, XRD, Raman and FTIR. The BET, SEM and XRD results showed that the Ash/mineral matter is associated with coal, carbon forms the main structural framework and mineral matters are found embedded in the coal structure in the low-rank tri-high coal. The Raman and FTIR results show that the ash can hinder volatile matters from exposing to the coal particles. Those results indicate that the surface of AFC chars has more free active carbon sites than raw coal chars, which are favorable for mass transfer between C and CO_2, thereby improving reactivity of the AFC chars. However, the gasification reactivity was dominated by pore structure at elevated gasification temperatures, even though the microcrystalline structure, functional group structure, and increase in the disorder carbon were improved by acid pickling.

Keywords: ash-free coal; CO_2 gasification; coal structure; tri-high coal

1. Introduction

Excessive carbon dioxide emissions have caused serious environmental problems, especially for global warming [1]. Synthetic gas (H_2 + CO) via gasification is the most important intermediate product in the highly efficient technologies [2,3]. Steam and carbon dioxide (CO_2) are two regular gasification agents and can usually control the overall conversation process [4]. Although it has been widely used as a gasification agent, CO_2 gasification is important as it is the slowest among gasification reactions and considered as the rate determining step, as well as the key to making a balance between air or oxygen and steam to generate optimum heat for driving endothermic gasification reactions [5,6]. The process of coal CO_2 gasification can be divided into pyrolysis and char gasification reaction [7], and the char gasification formed in situ from pyrolysis process is the rate-determining step [8]. Therefore, the kinetics of char gasification are vital in the design and operation of the gasifier. The gasification of tri-high coal chars often proceeds under the effect of the mineral content in particular, by significantly affecting the gasification rate, which will complicate the kinetics [9,10]. There are several combined chemical and physical steps involved in the conversion rate of coal char [11–14], such as the external mass transfer, inter-particle diffusion and surface reactions. All these steps are associated with changes in the pore structure and the chemical composition of the coal char. However, in some conditions, with the effects of high-ash contents on the chemical composition and porous structure during coal

gasification, the gasification characteristics will vary significantly. In southwest of China, tri-high coal, as the most representative type of coal, is characterized by high-ash content, high-sulfur content and high-ash fusion, which will limit its use in gasification process. However, it is uncertain whether the existing environment of ash is really a factor determining the rate of gasification [15]. In our previous work [3], the derivations and variations of char structures throughout the char gasification process were studied, indicating that both of the porous structure and carbon crystallites can affect the char CO_2 gasification kinetics [16].

The most reasonable way to quantify the influence of mineral content on the char gasification kinetics and its relationship with the initial coal structure is to remove the mineral content from the coal (named ash-free coal), and then investigate the gasification characteristics and structures of the ash-free coal [17–19]. There are two methods of char preparation to investigate the influence of mineral content on the char gasification: (1) removal of mineral content by pickling of char derived from pyrolysis, and (2) pyrolysis of coal, of which mineral content has been removed by pickling or other methods [20–22]. However, coal pyrolysis is the initial stage of coal gasification, and closely related to coal composition and structure, which will significantly affect the char gasification characteristics. The mineral content has a great influence on the formation of coal char, such as the cracking of organic matter in coal, volatilization of low-molecular-weight pyrolysis products, polycondensation of cracking residues, decomposition and combination of volatile products during emission, and further decomposition and repolycondensation of the polycondensation products during the pyrolysis process. The composition and structure of coal are directly related to the coal gasification kinetics [9,10,23]. Thus, the method (2) was chosen to produce ash-free coals (AFCs) in this research.

In this paper, two tri-high coals were selected to remove mineral contents by pickling method. The CO_2 gasification characteristics of raw coals and ash-free coals were investigated by using a thermo-gravimetric analyzer. Meanwhile, the structure of the raw coals (RCs), ash-free coals (AFCs) and their chars were characterized by SEM, BET, XRD, Raman and FTIR spectroscopy. The specific method can be obtained in our previous work [3].

2. Materials and Methods

2.1. Materials

Two tri-high coal samples were collected for the experiments from Guizhou Province in southwest of China. The AFC samples were produced by acid pickling. The nitric acid solution was added to the RC at a solution to coal ratio of 20:1 by weight, and the slurry was stirred for 24 h to ensure the coal wetting. After filtration, the filtered coal was mixed with hydrofluoric acid, and then stirred for 24 h and again filtered. Mixing with deionized water, stirring and filtering were repeated until the PH = 7 to ensure complete removal of coal ash. All the agents used above were analytical reagents and the concentration was not diluted. For comparison, the RCs with similar particle size to the AFCs (75–106 μm) were used as well. The char was prepared at 950 °C under a nitrogen atmosphere in a horizontal tubular furnace. During the char preparation process, approximately 20 g coal was placed in a corundum crucible, and then heated at 20 °C/min to the designed temperature under a nitrogen atmosphere. Finally, the sample was held at 950 °C for 30 min. The proximate and ultimate analyses of the AFCs and the corresponding RCs are summarized in Table 1.

On a dry basis, RC-I and AFC-I samples had 9.42 wt.% and 13.67 wt.% of volatile, respectively, while RC-II and AFC-II samples had 13.79 wt.% and 52.34 wt.% of volatile, respectively. The ash contents of RC-I, AFC-I, RC-II and AFC-II were 21.45 wt.%, 0.19 wt.%, 25.26 wt.% and 0.16 wt.%, respectively. The increased Fixed carbon of AFC-I was consistent with the result of Rubiera et al. [24], while that of AFC-II decreased. This probably due to the nitric acid showing poor effect on the mineral content, hydrofluoric acid dominated the acid pickling process. In addition, nitric acid played a role of oxidizing agent led to the increase in O content after pickling.

Table 1. Proximate and ultimate analysis of raw coals and ash-free coals.

Sample	Proximate Analysis (wt.%, db)			Ultimate Analysis (wt.%, daf)				
	Fixed Carbon	Volatile	Ash	C	H	N	O [a]	S
RC-I	69.13	9.42	21.45	89.2	2.25	0.52	5.56	2.47
AFC-I	86.14	13.67	0.19	88	1.76	1.01	8.39	0.84
RC-II	60.95	13.79	25.26	86.95	3.73	1.89	5.12	2.31
AFC-II	47.5	52.34	0.16	71.01	2.65	5.33	20.28	0.73

db, dry basis; and daf, dry and ash-free; [a], oxygen content by difference.

2.2. CO_2 Gasification

Coal gasification consists of both the coal pyrolysis and char gasification. Meanwhile, char plays a role in the rate-determining step, because of its much lower speed than that of coal pyrolysis, throughout the coal gasification process. STA449F3 thermo-gravimetric analyzer (TGA) was used for the char gasification. To evaluate the gasification efficiency, Equation (1) was proposed to calculate the carbon conversion.

$$x = \frac{m_0 - m_t}{m_0 - m_{ash}}, \quad (1)$$

where m_0 and m_t are the initial char mass and the instantaneous char mass at reaction time t, respectively, and m_{ash} is the mass of the ash.

2.3. Sample Characterization

The BET was employed to obtain the specific surface areas and pores volumes. The crystallization phase and components of the samples were detected by X-ray diffraction (XRD). Thermo Scientific DXR Raman spectrometer and FTIR spectrometer were applied to determine the band positions, intensities, widths and areas. The specific method was referred to our previous work [3].

3. Results and Discussion

3.1. Experimental Results

3.1.1. Gasification Characteristics

To investigate the influence of ash on the CO_2 gasification kinetics, TGA experiments were carried out at different temperatures (950 °C–1200 °C). The results showed that the temperature effects on the char gasification were straightforward, and the elevation of gasification temperature generally resulted in increased carbon conversion efficiency. Figure 1 also shows that the acid pickling was conducive to the CO_2 gasification. It was observed that the total conversion time of coal was shortened after ash removal. For example, the total conversion time of RC-I and AFC-I at 1150 °C was nearly 50 min and 30 min, respectively, while that of RC-II and AFC-II at 1150 °C was more than 80 min and nearly 5 min, respectively. It was illustrated that the existence of ash did have negative impacts on the gasification of coal char.

It is known that the particle size and the pore structure of the RC chars and AFC chars were not fixed. Therefore, with the purpose to quantitatively evaluate the reactivity of RC chars and AFC chars, the reactivity index $R_{0.5}$ ($R_{0.5} = 0.5/t_{50}$) [25] was used in this study, t_{50} is the time at which the carbon conversion reached 50%. The reactivity index for RC chars and AFC chars were shown in Figure 2. For all chars, it is obvious that the reactivity index $R_{0.5}$ increased with the gasification temperature. It suggests that the increasing gasification temperature is favor to the gasification reactivity. Furthermore, the reactivity index of RC-I char, AFC-I char, RC-II char, AFC-II char at temperatures of 950 °C–1200 °C were 0.0081–0.18182 min^{-1}, 0.01111–0.11905 min^{-1}, 0.00676–0.08264 min^{-1}, 0.06849–0.43478 min^{-1}, respectively. It can be seen that the $R_{0.5}$ of ARC-II was obviously higher than that of RC-II while the

AFC-I showed a contrary trend. In addition, the $R_{0.5}$ of AFC-I was similar to that of RC-I, and then the $R_{0.5}$ of RC-I was higher than that the former at elevated temperature.

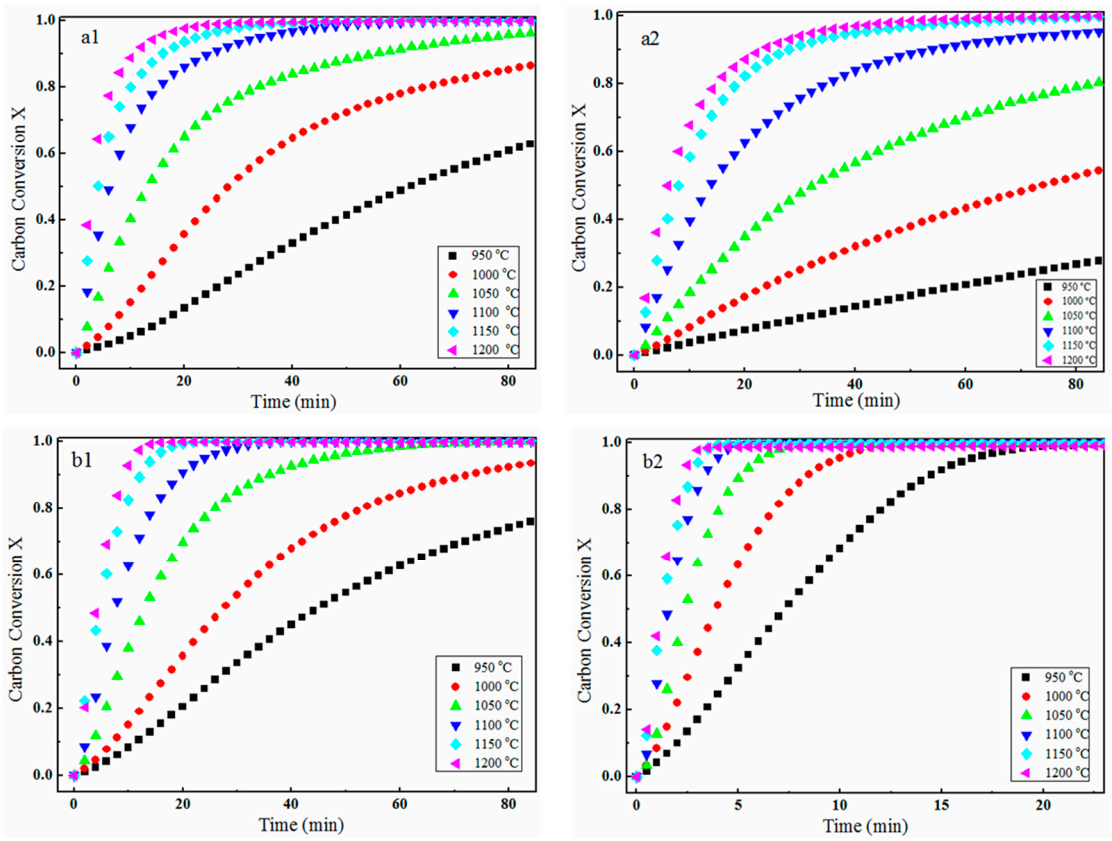

Figure 1. The profiles of carbon conversion vs. gasification time, in response to variation of the temperatures (**a1**: RC-I, **b1**: RC-II; **a2**: AFC-I; **b2**: AFC-II).

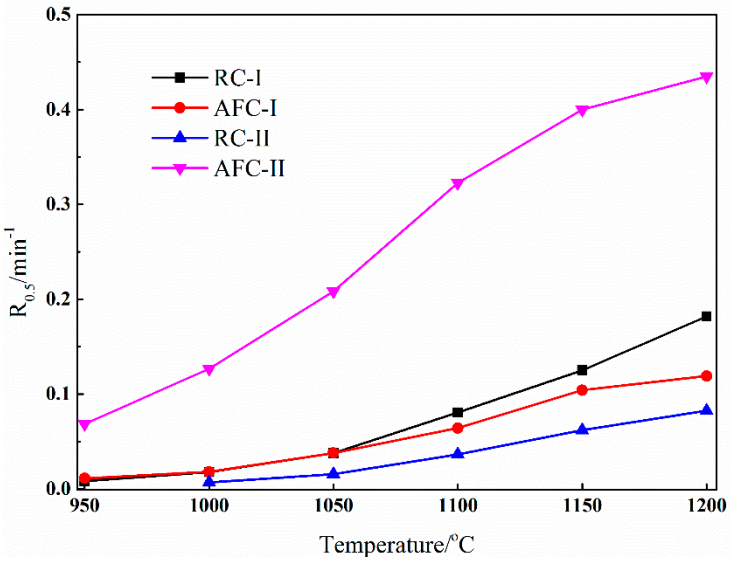

Figure 2. The reactivity index for raw coals (RCs), ash-free coals (AFCs).

The ash content has a great influence on the composition and structure of coal during the pyrolysis process, which is directly relative to the char gasification kinetics. Thus, the structure of the coal and char samples prepared at elevated temperatures and their influences on the gasification characteristics were studied in the next section.

3.1.2. Pore Structure

Measurements of BET specific surface area and total pore volume for the RCs, AFCs and their coal chars are presented in Table 2. Figure 3 shows the surface topography of each sample.

Table 2. BET surface areas and total pore volume of the selected samples.

Sample	RC-I	RC-I Char	AFC-I	AFC-I Char	RC-II	RC-II Char	AFC-II	AFC-II Char
BET surface area (m^2/g)	20.37	31.21	9.87	18.97	6.68	5.89	18.34	12.67
Total pore volume (ml/g)	0.043	0.083	0.023	0.042	0.030	0.021	0.050	0.043

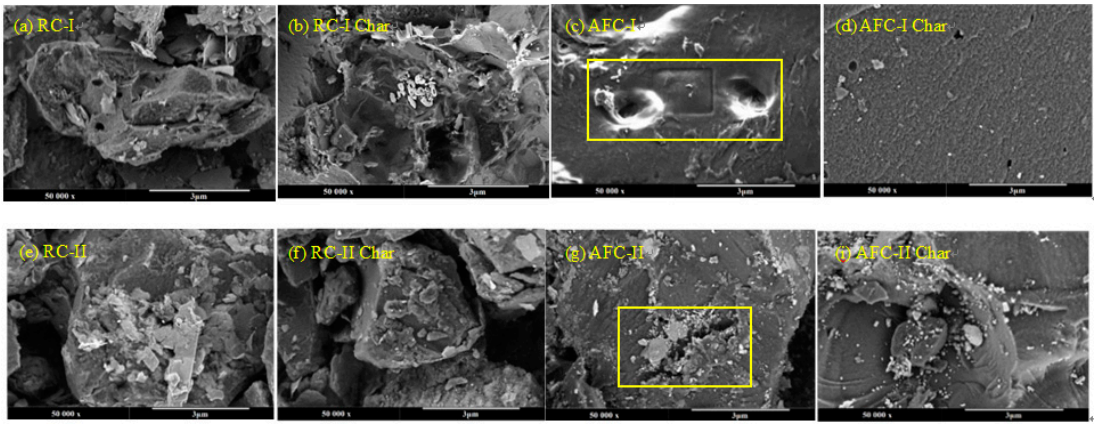

Figure 3. SEM of RCs, AFCs and their Chars (**a**–**d**: coal I, **e**–**i**: coal II).

Both the surface area and total pore volume of AFC-I were smaller than those of RC-I, which may result from the collapse of pore structure without ash embedded in the coal. Figure 3c reveals that the channels caused by pickling deeply penetrated into the sample surface, which means the ash is embedded in the coal and plays the role of skeleton of pore structure. In the research of Ni et al. [26], nitric acid can increase the surface area of coal, but nitric acid shows poor effect on the RC-I. Hydrofluoric acid removed the ash content and led to the collapse of RC-I pore structure. Therefore, the surface area and total pore volume of RC-I char were larger than those of AFC-I char, which is because the pore structure under sample surface may have been reserved when not to remove the ash. However, the surface area and total pore volume of RC-II and AFC-II were opposite compared with RC-I and AFC-I. Figure 3g illustrates that RC-II has a more stable structure, and ash removal contributes to the pore development, which is absolutely different with RC-I. The ash dissolution produced a large amount of pores during acid pickling [26], which resulted in an increase in surface area for AFC-II char. The larger surface area promoted the mass transfer of CO_2; therefore, the carbon conversion of AFC-II was significantly higher than that of RC-II. However, the conversion of AFC-I was lower than that of RC-I because of the surface area was decreased.

3.1.3. XRD Patterns Analysis

The XRD patterns and crystalline structure of RCs, AFCs and their chars are shown in Figure 4 and Table 3, respectively. It was noted that no ash content was detected in the AFCs and their chars, indicating the ash content was absolutely removed. The presence of a clear (002) band at ~26° and (100) band in the neighborhood of the graphite at ~43° suggested the existence of some graphite-like structures (crystalline carbon) in RCs and AFCs, as shown in Figure 4, which indicated that the crystallites in the samples had intermediate structures between graphite and the amorphous state. The presence of the clear asymmetric (002) band around 26° suggested the existence of another band (γ) on its left-hand side, which was attached to the periphery of carbon crystallites. It was observed that the γ peaks of RCs decreased after pickling, meaning that pickling contributes to the crack of aliphatic side chains.

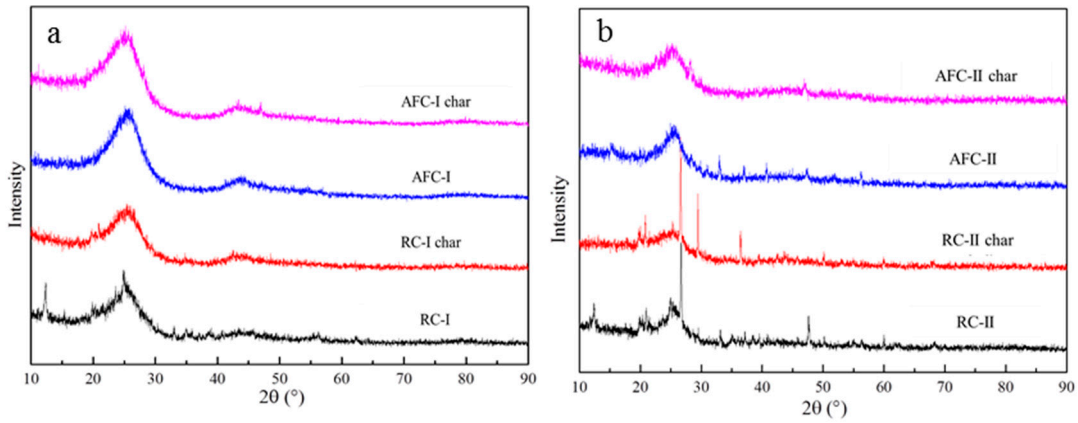

Figure 4. XRD patterns of RCs, AFCs and their Chars ((**a**): I, (**b**): II).

Table 3. Crystalline structure fitting results of RCs, AFCs and their Chars.

Sample	d_{002} (Å)	L_c (Å)
RC-I	3.52	3.066
RC-I Char	3.50	3.229
AFC-I	3.48	3.370
AFC-I Char	3.53	3.107
RC-II	3.49	4.335
RC-II Char	3.53	3.770
AFC-II	3.55	3.516
AFC-II Char	3.49	3.159

Compared with RC-I, the graphite layer spacing of AFC-I was decreased, while the crystal thickness rose. It indicated the presence of minerals between graphite layers. When acid pickling was executed to remove the ash, condensation of graphite layers occurred, which is consistent with the BET and SEM results. Compared with RC-II, the graphite layer spacing of AFC-II rose, while the vertical dimension (L_c) width decreased. AFC-II and its char have more disordered microcrystalline structures than RC-II and its chars. This may be because the fracture effect of the graphite layer produced much smaller layers during removing the ash in the layers by combining analysis with the BET and SEM results. Meanwhile, decomposition products of aromatic lamellar lubricated the fractured graphite layers, which resulted in the graphite layer spacing of AFC-II rising. Meanwhile, the microcrystalline structures of RC-II, AFC-II and their char were more ordered than those of RC-I, AFC-I and their chars.

3.1.4. Raman Spectra Analysis

The typical first-order region Raman spectra profile between 800 and 2000 cm^{-1} of the selected sample are shown in Figure 5. Figure 5 exhibits two characteristic peaks at ~1330 cm^{-1} (D band) and ~1590 cm^{-1} (G band) in Raman spectra [27]. The Raman spectra were subjected to peak fitting using a curve fitting software, Peakfit4.2, to resolve the spectra into three Lorentzian bands (designated as the G, D_1 and D_4 bands, respectively) and one Gaussian band (for the D_3 band), as shown in Figure 5. The D_1 band at ~1350 cm^{-1} is the broadening of the G peak resulting from the introduced disorder carbon, the D_3 band at ~1500 cm^{-1} refers to the amorphous sp^2-bonded forms of carbon, D_4 at ~1250 cm^{-1} is considered to be caused by the amorphous mixed sp^2-sp^3 bonded forms of carbon, and G band refers to graphitic band [28–30].

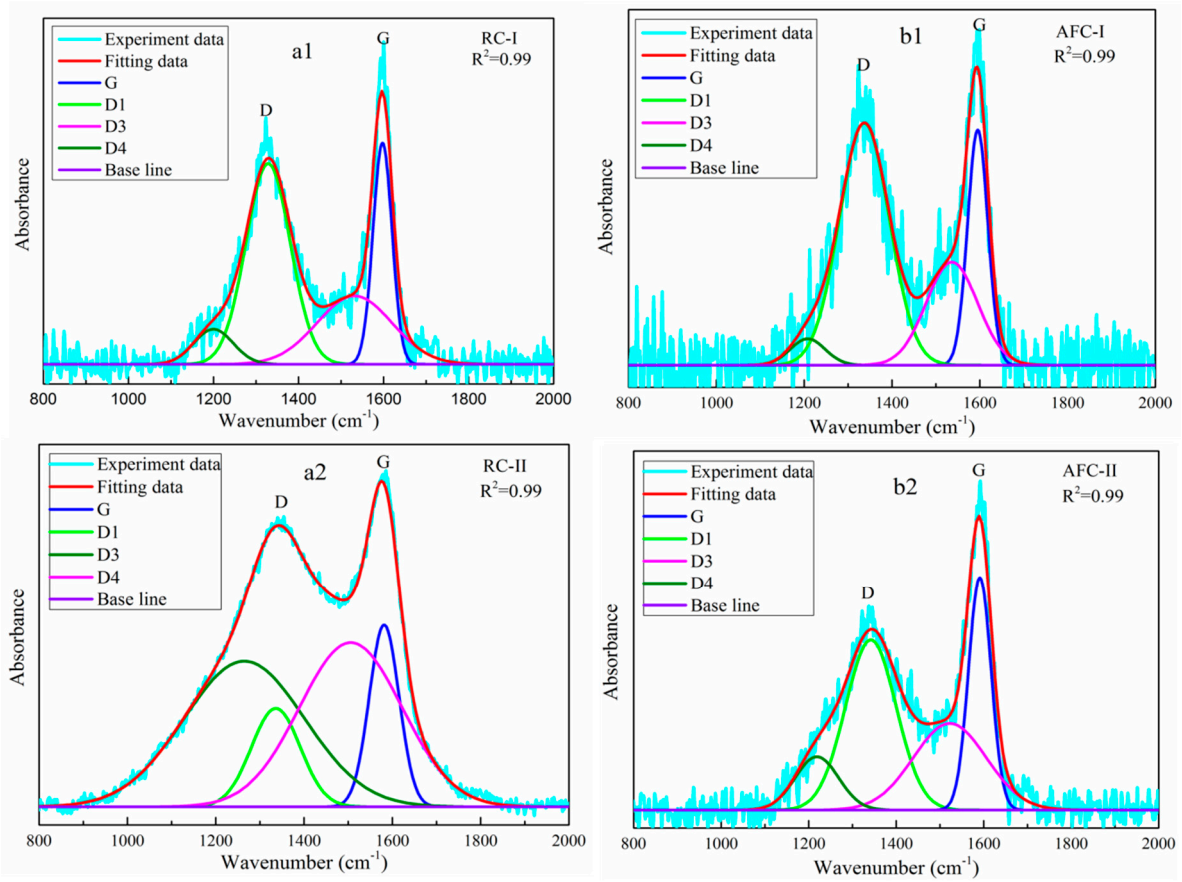

Figure 5. Typical first-order region Raman spectra and the bands of the selected samples (**a1**: RC-I; **b1**: AFC-I; **a2**: AFC-I; **b2**: AFC-II).

The band area ratios of the D_1, D_3 and D_4 to the G (denoted as I_{D1}/I_G, I_{D3}/I_G and I_{D4}/I_G) and the G band relative to the integrated area under the spectra (denoted as I_G/I_{All}) of each sample are shown in Table 4. Compared with the RCs, the I_{D1}/I_G of the AFC chars increased, indicating that the acid pickling removed the ash is not conducive to the orderly development of RCs [31]. The ratios of I_{D3}/I_G and I_{D4}/I_G of AFC chars were less than those of the RC chars, which was due to the hydrolysis of small aromatic structures to aromatic C=C and some aliphatic groups to C–O in phenols, alcohols, ethers and esters bands, decreasing the relative contents of sp^2 and sp^2-sp^3 bonding carbon atoms in AFC chars. The gasification reactivity of RC-I and RC-II was improved by the acid pickling due to more disordered carbon forming and being exposed to the surface.

Table 4. I_{D1}/I_G, I_{D3}/I_G, I_{D4}/I_G and I_G/I_{All} of each sample.

Sample	I_{D1}/I_G	I_{D3}/I_G	I_{D4}/I_G	I_G/I_{All}
RC-I	1.72	0.91	0.49	24.24
RC-I char	2.12	1.22	0.33	21.43
AFC-I	2.03	0.79	0.26	24.5
AFC-I char	2.54	1.11	0.19	20.62
RC-II	1.43	1.64	0.95	19.75
RC-II char	0.88	3.09	3.23	12.19
AFC-II	1.98	1.2	0.35	22.03
AFC-II char	1.66	1.21	0.44	23.23

3.1.5. FTIR Spectra Analysis

FTIR was carried out to understand the carbon functional groups of the selected samples, and the FTIR spectra are shown in Figure 6. The spectra showed six principal bands at 3900–3200 cm^{-1}, 3200–3000 cm^{-1}, 2960–2850 cm^{-1}, 1630–1540 cm^{-1}, 1390 cm^{-1}, 1250–1000 cm^{-1} and 900–700 cm^{-1}, respectively. The bands at 3900–3200 cm^{-1} were assigned to –OH stretching and organic compounds having oxygen functional groups found in coal including phenols, alcohols and carboxylic acid, the bands between 3150 and 3000 cm^{-1} were assigned to C–H bonds in aromatics, the bands at 2960–2850 cm^{-1} were assigned to aliphatic C–H stretching, the bands at 1630–1540 cm^{-1} were assigned to aromatic C=C stretching, the bands at ~1400 cm^{-1} to aliphatic $–CH_3$ bending, the bands between 1250 and 1000 cm^{-1} were assigned to C–O in phenols, alcohols, ethers and esters, and the bands between 900 and 700 cm^{-1} were assigned to aromatic out-of-plane C–H bending [29,32–34].

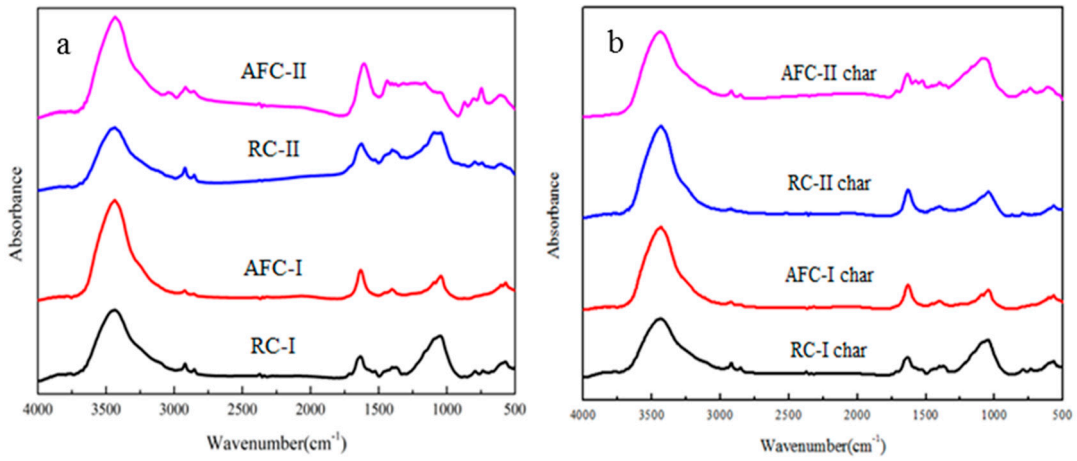

Figure 6. FTIR spectra of the selected samples ((**a**): raw coals, (**b**): chars).

The fitted FTIR spectra of the samples at the selected regions (4000–2600 cm^{-1} and 1800–650 cm^{-1}) are shown in Figure 7, and the band ratios of the samples at each region are shown in Table 5. For the range of 4000–2600 cm^{-1}, there was a short and narrow absorption above 3600 cm^{-1} in all of the samples, suggesting that free hydroxyl groups exist in the samples. It was also observed that there was a broad and strong absorption peak at ~3450 cm^{-1} in the samples, which is assigned to hydrogen-bonded hydroxyl group vibrations (poly –OH1). The absorption at ~3210 cm^{-1} assigned to wagging vibrations of hydroxyl group (poly –OH2) was also present. Owing to the loss of a part of hydroxyl groups (poly –OH1 and –OH2) dissolved in acid solution, the hydroxyl group ratios between two AFCs were lower than those of the corresponding RCs, and the relative content of aromatic C–H was increased. However, the band ratios of aliphatic C–H between 2960 and 2850 cm^{-1} of the two AFCs decreased, which was due to the reactions between acid solution and ash in coals during the acid pickling process, which releases a lot of heat, resulting in the cracking of aliphatic C–H to low-molecular-weight groups, such as C–O in phenols, alcohols, ethers and esters.

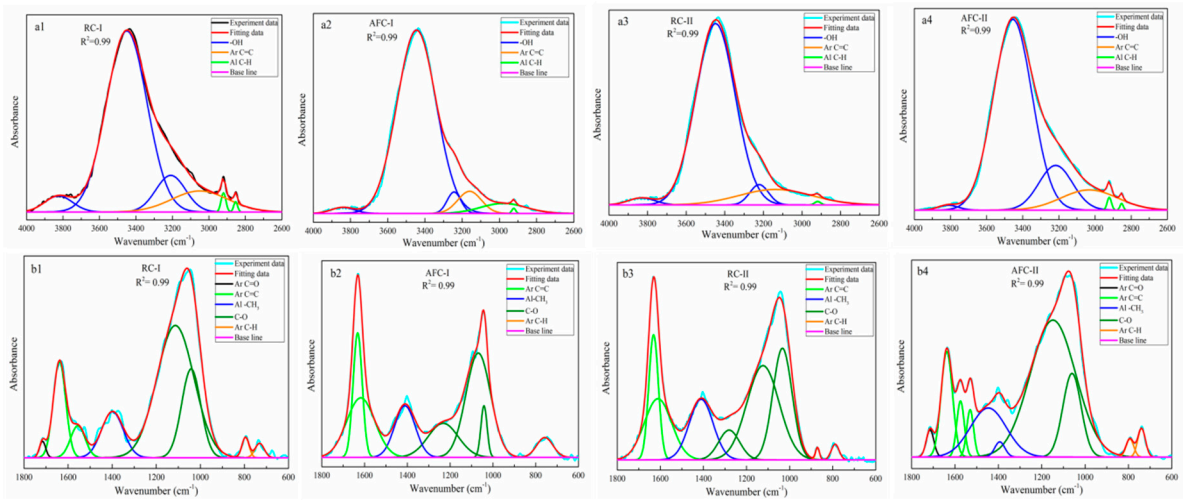

Figure 7. Infrared spectra of selected samples with the corresponding curve fitted bands in the ranges 4000–2600 cm^{-1} (**a_1**–**a_4**) and 1800–650 cm^{-1} (**b_1**–**b_4**); Ar, aromatic and Al, aliphatic.

Table 5. The band ratios of the samples at each region (%, dry basis).

Range, cm^{-1}	Band Position, cm^{-1}	Sample							
		RC-I	**RC-I Char**	**AFC-I**	**AFC-I Char**	**RC-II**	**RC-II Char**	**AFC-II**	**AFC-II Char**
4000–2600	poly –OH (~3400–3200)	82.67	87.42	80.67	86.31	96.02	87.04	81.32	88.12
	aromatic C–H (3150–3000)	16.08	11.58	18.57	13.37	-	12.72	17.28	11.13
	aliphatic C-H (2960–2850)	1.25	1.28	0.76	0.32	3.98	0.24	1.44	0.75
1800–600	aromatic carboxyl C=O (1710)	2.46	1.06	1.13	-	-	-	-	1.7
	aromatic C=C (1630–1440)	16.95	17.25	28.19	34.53	21.62	27.94	23.99	16.05
	aliphatic $–CH_3$ (~1400)	10.56	10.38	6.25	13.09	20.56	14.03	12.22	1.27
	C-O (1250–1050)	66.83	68.45	61.29	48.41	51.73	56.38	63.79	78.16
	aromatic C–H (700–900)	3.2	3.86	3.13	3.97	6.09	1.65	5.21	2.92

For the range 1800–600 cm^{-1}, more aromatic C=C is exposed to the surface of particles via acid pickling, which results in a higher aromatic C=C ratio of AFC-I char than that of RC-I char. More aliphatic groups are also exposed to the particle surface via acid pickling, but some of aliphatic groups crack to small molecular structure under heat produced from the reactions between acid solution and ash, which results in a lower band ratio of aliphatic groups of AFC-I than that of RC-I. However, a higher band ratio of aliphatic $–CH_3$ of AFC-I char than that of RC-I char was obtained after devolatilization, and the band ratio of low-molecular-weight group C-O was greatly reduced.

More aromatic and aliphatic groups are also exposed to the particle surface of particles via acid pickling, which results in a higher aromatic ratio of AFC-II than that of RC-II. Meanwhile, acid pickling produced more structure defects, leading to much easier cracking of aromatic C=C and aliphatic $–CH_3$ to low-molecular-weight group C–O. Thus, the band ratio of aromatic C=C and aliphatic $–CH_3$ of AFC-II char was lower than that of RC-II char, and the band ratio of low-molecular-weight group C–O of AFC-II was higher than that of RC-II.

In brief, the lower rank the coal is, the more volatile matters will be hindered by the ash while exposed to the coal particle surface.

4. Conclusions

Two kinds of tri-high coals were studied to determine the influence of ash-existing environments on CO_2 gasification characteristics. The results illustrated that the ash embedded in high rank tri-high coal. The ash usually hinders volatile matter exposed to the surface of coal particles. Acid pickling could improve the microcrystalline structure and functional group structure, and increase the disorder carbon, but the gasification reactivity was also dominated by pore structure at elevated gasification temperatures. The lower the rank the tri-high coal is, the more obstruction effects the ash has. In other words, removing the ash of the low rank tri-high coal can help to promote CO_2 gasification efficiency.

Author Contributions: L.L.: Conception, editing, obtain research funding; Q.J.: Experiment, data analysis, editing; B.K.: Experiment, data analysis; J.Y., S.R., Q.L.: Conception, writing review. All authors have read and agreed to the published version of the manuscript.

Funding: This study was supported by the Science and Technology Planning Project of Guizhou province (Qiankehejichu [2018]1066), Young Teachers Training Project of Guizhou Institute of Technology ([2017]5789-05), Guizhou Science and Technology Support Project (Contract no: Qiankehe Zhicheng [2019]2872) and the Research Start-up Funding Project for High-level Talents of Guizhou Institute of Technology.

Conflicts of Interest: The authors declare no conflict of interest.

References

1. Ren, S.; Aldahri, T.; Liu, W.; Liang, B. CO_2 mineral sequestration by using blast furnace slag: From batch to continuous experiments. *Energy* **2021**, *214*, 118975. [CrossRef]
2. Pérez-Fortes, M.; Bojarski, A.D.; Velo, E.; Nougués, J.M.; Puigjaner, L. Conceptual model and evaluation of generated power and emissions in an IGCC plant. *Energy* **2009**, *34*, 1721–1732. [CrossRef]
3. Liu, L.; Cao, Y.; Liu, Q. Kinetics studies and structure characteristics of coal char under pressurized CO_2 gasification conditions. *Fuel* **2015**, *146*, 103–110. [CrossRef]
4. Wang, M.; Zhang, J.; Zhang, S.; Wu, J.; Yue, G. Experimental studies on gasification of the Shenmu coal char with CO 2 at elevated pressures. *Korean J. Chem. Eng.* **2008**, *25*, 1322–1325. [CrossRef]
5. Huo, W.; Zhou, Z.; Chen, X.; Dai, Z.; Yu, G. Study on CO_2 gasification reactivity and physical characteristics of biomass, petroleum coke and coal chars. *Bioresour. Technol.* **2014**, *159*, 143–149. [CrossRef] [PubMed]
6. Nowicki, L.; Siuta, D.; Markowski, M.J.E. Carbon Dioxide Gasification Kinetics of Char from Rapeseed Oil Press Cake. *Energies* **2020**, *13*, 2318. [CrossRef]
7. Kang, T.J.; Park, H.; Namkung, H.; Xu, L.H.; Fan, S.; Kim, H.T. Comparison of catalytic pyrolysis and gasification of Indonesian low rank coals using lab-scale bubble fluidized-bed reactor. *Korean J. Chem. Eng.* **2017**, *34*, 1238–1249. [CrossRef]
8. Sawettaporn, S.; Bunyakiat, K.; Kitiyanan, B.J. CO_2 gasification of Thai coal chars: Kinetics and reactivity studies. *Korean J. Chem. Eng.* **2009**, *26*, 1009–1015. [CrossRef]
9. Franklin, H.D.; Peters, W.A.; Howard, J.B. Mineral matter effects on the rapid pyrolysis and hydropyrolysis of a bituminous coal: 2. Effects of yields of C3-C8 hydrocarbons. *Fuel* **1981**, *61*, 1213–1217. [CrossRef]
10. Ehrburger, P.; Addoun, F.; Donnet, J.B. Effect of mineral matter of coals on the microporosity of charcoals. *Fuel* **1988**, *67*, 1228–1231. [CrossRef]
11. Lin, L.; Strand, M. Investigation of the intrinsic CO_2 gasification kinetics of biomass char at medium to high temperatures. *Appl. Energy* **2013**, *109*, 220–228. [CrossRef]
12. Ion, I.V.; Popescu, F.; Rolea, G.G. A biomass pyrolysis model for CFD application. *J. Therm. Anal. Calorim.* **2013**, *111*, 1811–1815. [CrossRef]
13. Tomaszewicz, M.; Łabojko, G.; Tomaszewicz, G.; Kotyczka-Morańska, M. The kinetics of CO_2 gasification of coal chars. *J. Therm. Anal. Calorim.* **2013**, *113*, 1327–1335. [CrossRef]
14. Fan, D.; Zhu, Z.; Na, Y.; Lu, Q. Thermogravimetric analysis of gasification reactivity of coal chars with steam and CO2 at moderate temperatures. *J. Therm. Anal. Calorim.* **2013**, *113*, 599–607. [CrossRef]
15. Feng, B.; Bhatia, S.K. Variation of the pore structure of coal chars during gasification. *Carbon* **2003**, *41*, 507–523. [CrossRef]

16. Yoon, S.P.; Deng, L.; Namkung, H.; Fan, S.; Kang, T.J.; Kim, H.T. Coal structure change by ionic liquid pretreatment for enhancement of fixed-bed gasification with steam and CO_2. *Korean J. Chem. Eng.* **2017**, *35*, 445–455. [CrossRef]
17. Kopyscinski, J.; Habibi, R.; Mims, C.A.; Hill, J.M. K_2CO_3-Catalyzed CO_2 gasification of ash-free coal: Kinetic study. *Energy Fuels* **2013**, *27*, 4875–4883. [CrossRef]
18. Wu, X.; Jie, W. K_2CO_3-catalyzed steam gasification of ash-free coal char in a pressurized and vertically blown reactor. Influence of pressure on gasification rate and gas composition. *Fuel Process. Technol.* **2017**, *159*, 9–18. [CrossRef]
19. Sharma, A.; Saito, I.; Takanohashi, T. Catalytic Steam Gasification Reactivity of HyperCoals Produced from Different Rank of Coals at 600–775 °C. *Energy Fuels* **2008**, *22*, 3561–3565. [CrossRef]
20. Kong, Y.; Kim, J.; Chun, D.; Lee, S.; Rhim, Y.; Lim, J.; Choi, H.; Kim, S.; Yoo, J. Comparative studies on steam gasification of ash-free coals and their original raw coals. *Int. J. Hydrog. Energy* **2014**, *39*, 9212–9220. [CrossRef]
21. Kim, J.; Choi, H.; Lim, J.; Rhim, Y.; Chun, D.; Kim, S.; Lee, S.; Yoo, J. Hydrogen production via steam gasification of ash free coals. *Int. J. Hydrog. Energy* **2013**, *38*, 6014–6020. [CrossRef]
22. Wu, X.; Jia, T.; Jie, W. A new active site/intermediate kinetic model for K_2CO_3-catalyzed steam gasification of ash-free coal char. *Fuel* **2016**, *165*, 59–67. [CrossRef]
23. Ellis, N.; Masnadi, M.S.; Roberts, D.G.; Kochanek, M.A.; Ilyushechkin, A.Y. Mineral matter interactions during co-pyrolysis of coal and biomass and their impact on intrinsic char co-gasification reactivity. *Chem. Eng. J.* **2015**, *279*, 402–408. [CrossRef]
24. Rubiera, F.; Arenillas, A.; Arias, B.; Pis, J.J.; Suarez-Ruiz, I.; Steel, K.M.; Patrick, J.W.J. Combustion behaviour of ultra clean coal obtained by chemical demineralisation. *Fuel* **2003**, *82*, 2145–2151. [CrossRef]
25. Takarada, T.; Tamai, Y.; Tomita, A.J. Reactivities of 34 coals under steam gasification. *Fuel* **1985**, *64*, 1438–1442. [CrossRef]
26. Ni, G.; Li, S.; Rahman, S.; Xun, M.; Wang, H.; Xu, Y.; Xie, H. Effect of nitric acid on the pore structure and fractal characteristics of coal based on the low-temperature nitrogen adsorption method. *Powder Technol.* **2020**, *367*, 506–516. [CrossRef]
27. Bai, Y.; Wang, Y.; Zhu, S.; Fan, L.I.; Xie, K. Structural features and gasification reactivity of coal chars formed in Ar and CO_2 atmospheres at elevated pressures. *Energy* **2014**, *74*, 464–470. [CrossRef]
28. Liu, X.; Ying, Z.; Liu, Z.; Ding, H.; Huang, X.; Zheng, C.J. Study on the evolution of the char structure during hydrogasification process using Raman spectroscopy. *Fuel* **2015**, *157*, 97–106. [CrossRef]
29. Cole-Clarke, P.A.; Vassallo, A.M. Infrared emission spectroscopy of coal. *Fuel* **1992**, *71*, 469–470. [CrossRef]
30. Chabalala, V.P.; Wagner, N.; Potgieter-Vermaak, S.J. Investigation into the evolution of char structure using Raman spectroscopy in conjunction with coal petrography; Part 1. *Fuel Process. Technol.* **2011**, *92*, 750–756. [CrossRef]
31. Yu, J.; Guo, Q.; Ding, L.; Gong, Y.; Yu, G. Studying effects of solid structure evolution on gasification reactivity of coal chars by in-situ Raman spectroscopy. *Fuel* **2020**, *270*, 117603. [CrossRef]
32. Sonibare, O.O.; Haeger, T.; Foley, S.F. Structural characterization of Nigerian coals by X-ray diffraction, Raman and FTIR spectroscopy. *Energy* **2010**, *35*, 5347–5353. [CrossRef]
33. Sharma, R.K.; Wooten, J.B.; Baliga, V.L.; Lin, X.; Geoffrey Chan, W.; Hajaligol, M.R. Characterization of chars from pyrolysis of lignin. *Fuel* **2004**, *83*, 1469–1482. [CrossRef]
34. Zhang, Y.; Kang, X.; Tan, J.; Frost, R.L. Influence of Calcination and Acidification on Structural Characterization of Anyang Anthracites. *Energy Fuels* **2013**, *27*, 7191–7197. [CrossRef]